

Investigating the role of background and observation error correlations in improving a model forecast of forest carbon balance using four dimensional variational data assimilation.

Ewan M. Pinnington^{a,*}, Eric Casella^c, Sarah L. Dance^{a,b}, Amos S. Lawless^{a,b}, James I. L. Morison^c, Nancy K. Nichols^{a,b}, Matthew Wilkinson^c, Tristan L. Quaife^{a,d}

^a*Department of Meteorology, University of Reading, Reading, UK*

^b*Department of Maths and Statistics, University of Reading, Reading, UK*

^c*Centre for Sustainable Forestry and Climate Change, Forest Research, Alice Holt, Farnham, UK*

^d*National Centre for Earth Observation, University of Reading, Reading, UK*

Abstract

Efforts to implement variational data assimilation routines with functional ecology models and land surface models have been limited, with sequential and Markov chain Monte Carlo data assimilation methods being prevalent. When data assimilation has been used with models of carbon balance, background “prior” errors and observation errors have largely been treated as independent and uncorrelated. Correlations between background errors have long been known to be a key aspect of data assimilation in numerical weather prediction. More recently, it has been shown that accounting for correlated observation errors in the assimilation algorithm can considerably improve data assimilation results and forecasts. In this paper we implement a Four-Dimensional Variational data assimilation (4D-Var) scheme with a simple model of forest carbon balance, for joint parameter and state estimation and assimilate daily observations of Net Ecosystem CO₂ Exchange (NEE) taken at the Alice Holt forest CO₂ flux site in Hampshire, UK. We then investigate the effect of specifying correlations between parameter and state variables in background error statistics and the effect of specifying correlations in time between observation error statistics. The idea of including these correlations in time is new and has not been previously explored in carbon balance model data assimilation. In data assimilation, background and observation error statistics are often described by the background error covariance matrix and the observation error covariance matrix. We outline novel methods for creating correlated versions of these matrices, using a set of previously postulated dynamical constraints to include correlations in the background error statistics and a Gaussian correlation function to include time correlations in the observation error statistics. The methods used in this paper will allow the inclusion of time correlations between many different observation types in the assimilation algorithm, meaning that previously neglected information can be accounted for. In our experiments we compared the results using our new correlated background and observation error covariance matrices and those using diagonal covariance matrices. We found that using the new correlated matrices reduced the root mean square error in the 14 year forecast of daily NEE by 44% decreasing from 4.22 gCm⁻²day⁻¹ to 2.38 gCm⁻²day⁻¹.

*Corresponding author

Email address: e.m.pinnington@pgr.reading.ac.uk (Ewan M. Pinnington)

Keywords: Data assimilation, Carbon cycle, DALEC, Eddy covariance, Observation error covariance, Background error covariance, Ecosystem modelling, Augmented state, Parameter estimation

1. Introduction

The land surface and oceans are responsible for removing around half of all human emitted carbon-dioxide from the atmosphere and therefore mediate the effect of anthropogenic induced climate change. Terrestrial ecosystem carbon uptake is the least understood process in the global carbon cycle (Ciais et al., 2014). It is therefore vital that we improve understanding of the carbon uptake of terrestrial ecosystems and their response to climate change in order to better constrain predictions of future carbon budgets. Observations of the Net Ecosystem Exchange (NEE) of CO₂ between terrestrial ecosystems and the atmosphere are now routinely made at flux tower sites world-wide, at sub-hourly resolution and covering multiple years (Baldocchi, 2008), providing a valuable resource for carbon balance model validation and data assimilation.

Data assimilation is the process of combining a mathematical model with observations in order to improve the estimate of the state of a system. Data assimilation has successfully been used in many applications to significantly improve model state and forecasts. Perhaps the most important application has been in numerical weather prediction where data assimilation has contributed to the forecast accuracy being increased at longer lead times, with the four day forecast in 2014 having the same level of accuracy as the one day forecast in 1979 (Bauer et al., 2015). This increase in forecast skill is obviously not solely due to data assimilation but also increased quality and resolution of observations along with improvements in model structure, however the introduction and evolution of data assimilation has played a large part (Dee et al., 2011). The current method implemented at many leading operational numerical weather prediction centres is known as Four-Dimensional Variational data assimilation (4D-Var) (Bonavita et al., 2015; Clayton et al., 2013), which has been shown to be a significant improvement over its predecessor three-dimensional variational data assimilation (Lorenc and Rawlins, 2005). Variational assimilation techniques minimise a cost function to find the optimal state of a system given all available knowledge of errors in the model and observations. The minimisation routine typically requires the derivative of the model which can sometimes prove difficult to calculate. Using techniques such as automatic-differentiation (Renaud, 1997) can reduce the time taken to implement the derivative of a model. In numerical weather prediction data assimilation has been predominately used for state estimation whilst keeping parameters fixed. Variational data assimilation can be used for joint parameter and state estimation by augmenting the state vector with the parameters (Navon, 1998). By including the parameters in the state vector we must also specify error statistics and error correlations for them. Smith et al. (2009) show that the prescription of these error statistics and their correlations can have a significant impact on parameter-state estimates obtained from the assimilation.

Many different observations relevant to the carbon balance of forests have now been combined with functional ecology models, using data assimilation, in order to improve our knowledge ecological systems (Zobitz et al., 2011; Fox et al., 2009; Richardson et al., 2010; Quaife et al., 2008; Zobitz et al., 2014; Niu et al., 2014). Two such models that have been used extensively with data assimilation are the Data Assimilation Linked Ecosystem Carbon (DALEC) model (Williams et al.,

2005) and the Simplified Photosynthesis and Evapo-Transpiration (SIPNET) model (Braswell et al., 2005). Nearly all data assimilation routines built with these models have used sequential and Monte Carlo Markov chain (MCMC) data assimilation methods with the exception of a variational routine being implemented for DALEC by Delahaies et al. (2013). There have been examples of global land surface models being implemented with variational methods such as the ORganizing Carbon and Hydrology In Dynamic Ecosystems model (ORCHIDEE) (Krinner et al., 2005) and the Biosphere Energy Transfer Hydrology scheme (BETHY) in a Carbon Cycle Data Assimilation System (CCDAS) (Kaminski et al., 2013). These examples have mainly been used to assimilate data from satellite and atmospheric CO₂ observations with only a few cases where site level data has also been assimilated (Verbeeck et al., 2011; Bacour et al., 2015).

Background errors (describing our knowledge of error in prior model estimates before data assimilation) and observation errors have largely been treated as uncorrelated and independent in ecosystem model data assimilation schemes. In 3D and 4DVar schemes background and observation errors are represented by the error covariance matrices **B** and **R** respectively. The off-diagonal elements of these matrices indicate the correlations between errors in the parameter and state variables for **B** and the correlations between observation errors for **R**. In the assimilation, the off-diagonal terms in the **B** matrix act to spread information between the state and augmented parameter variables (Kalnay, 2003). This means that assimilating observations of one state variable can act to update different state and parameter variables in the assimilation when correlations are included in **B**. In 4D-Var the **B** matrix is propagated implicitly by the forecast model, so that even a propagated diagonal **B** matrix can develop correlations throughout an assimilation window. These correlations will only be in the propagated **B** matrix, with the **B** matrix valid at the initial time remaining unchanged. Including correlations in **B** has been shown to significantly improve data assimilation results in numerical weather prediction (Bannister, 2008).

Including correlations between observation errors has only started to be explored recently in numerical weather prediction, with **R** still often treated as diagonal (Stewart et al., 2013). Including some correlation structure in **R** has been shown to improve forecast accuracy (Weston et al., 2014). Currently the correlations included in **R** have been mainly between observations made at the the same time rather than correlations between observations throughout time. When assimilating observations, data streams with many more observations can have a greater impact on the assimilation than those with fewer observations. In Richardson et al. (2010) this problem is discussed when assimilating large numbers of NEE observations along with smaller numbers of leaf area index and soil respiration observations. To address this problem Richardson et al. uses a cost function that calculates the product of the departures from the observations rather than a cost function which sums these departures, giving a relative rather than absolute measure of the goodness-of-fit to the observations. This problem is also encountered in Bacour et al. (2015) when assimilating daily eddy covariance data with weekly observations of the FrAction of Photosynthetically Active Radiation (FAPAR). In Bacour et al. (2015) the error in observations of FAPAR is divided by two in order to give these less frequent observations more weight in the assimilation algorithm. Specifying serial time correlations between observations represents another way of addressing this problem, whilst also adding valuable information to the data assimilation routine. Including serial correlations between observations of the same quantity decreases the impact of these

64 observations (Järvinen et al., 1999) therefore increasing the impact of less frequent observations.

65 In this paper we implement the new version of DALEC (DALEC2 (Bloom and Williams, 2015)) in a 4D-Var data assimilation scheme for joint state and parameter estimation, assimilating daily NEE observations from the Alice Holt flux site in
66 Hampshire, UK (Wilkinson et al., 2012). This assimilation scheme is then subjected to rigorous testing to ensure correctness.
67 A new method is outlined for including parameter and state correlations in the background error covariance matrix. Currently
68 parameter and state error statistics are largely treated as independent and uncorrelated when data assimilation has been used
69 with models of carbon balance. We also introduce a novel method for including serial time correlations in the observation
70 error covariance matrix. The idea of including time correlations between observation error statistics is new and has not been
71 previously explored in carbon balance model data assimilation. These correlated matrices are then used in a series of ex-
72 periments in order to examine the effect that including correlations in the assimilation scheme has on the results. We show
73 that specifying parameter and state correlations in the prior knowledge and serial correlations between observation errors can
74 significantly improve the fit of the predicted carbon balance to observations with the root mean square error in the 14 year
75 forecast of daily NEE decreasing by 44% from $4.22 \text{ gCm}^{-2}\text{day}^{-1}$ to $2.38 \text{ gCm}^{-2}\text{day}^{-1}$.
76

77 2. Model and Data Assimilation Methods

78 2.1. Alice Holt research forest

79 Alice Holt Forest is a research forest area managed by the UK Forestry Commission located in Hampshire, SE England.
80 Forest Research has been operating a CO₂ flux measurement tower in a portion of the forest, the Straits Inclosure, since
81 1998 so it is one of the longer forest site CO₂ flux records, globally. The Straits Inclosure is a 90ha area of managed
82 deciduous broadleaved plantation woodland, presently approximately 80 years old, on a surface water gley soil. The majority
83 of the canopy trees are oak (*Quercus robur* L.), with an understory of hazel (*Corylus avellana* L.) and hawthorn (*Crataegus*
84 *monogyna* Jacq.); but there is a small area of conifers (*Pinus nigra* J. F. Arnold) within the tower measurement footprint
85 area in some weather conditions. Further details of the Straits Inclosure site and the measurement procedures are given in
86 Wilkinson et al. (2012), together with analysis of stand-scale 30 minute average net CO₂ fluxes (NEE) measured by standard
87 eddy covariance methods from 1998-2011. The data used here span from January 1999 to December 2013, and consist of
88 the NEE fluxes and meteorological driving data of temperatures, irradiance and atmospheric CO₂ concentration. The original
89 NEE data were subjected to normal quality control procedures, including u^* filtering to remove unreliable data when there
90 were low turbulence night time conditions, as described in Wilkinson et al. (2012), but were not gap-filled. To compute
91 daily NEE observations we take the sum over the 48 measurements made each day. We only select days where there is no
92 missing data and over 90% of CO₂ flux observations have a quality control flag associated with the best observations and no
93 observations associated with the worst from the EddyPro flux processing software (LI-COR, Inc., 2015).

94 2.2. The DALEC2 model

95 The DALEC2 model is a simple process-based model describing the carbon balance of a forest ecosystem (Bloom and
 96 Williams, 2015) and is the new version of the original DALEC (Williams et al., 2005). The model is constructed of six carbon
 97 pools (labile (C_{lab}), foliage (C_f), fine roots (C_r), woody stems and coarse roots (C_w), fresh leaf and fine root litter (C_l) and soil
 98 organic matter and coarse woody debris (C_s)) linked via fluxes. The aggregated canopy model (ACM) (Williams et al., 1997)
 99 is used to calculate daily gross primary production (GPP) of the forest, taking meteorological driving data and the modelled
 100 leaf area index (a function of C_f) as arguments. Figure 1 shows a schematic of how the carbon pools are linked in DALEC2.

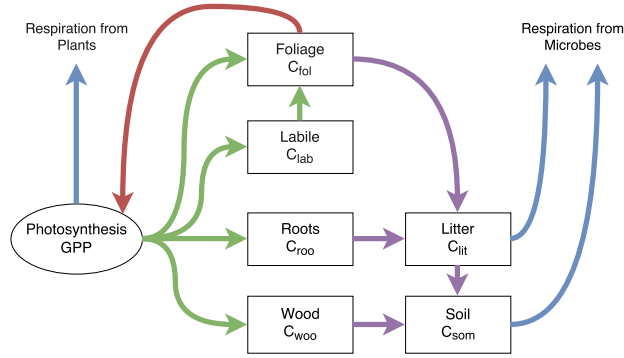


Figure 1: Representation of the fluxes in the DALEC2 carbon balance model. Green arrows represent C allocation, purple arrows represent litter fall and decomposition fluxes, blue arrows represent respiration fluxes and the red arrow represents the influence of leaf area index in the GPP function.

101 The model equations for the carbon pools at day i are as follows:

$$GPP^i = ACM(C_{fol}^{i-1}, c_{lma}, c_{eff}, \Psi) \quad (1)$$

$$C_{lab}^i = (1 - \Phi_{on})C_{lab}^{i-1} + (1 - f_{auto})(1 - f_{fol})f_{lab}GPP^i, \quad (2)$$

$$C_{fol}^i = (1 - \Phi_{off})C_{fol}^{i-1} + \Phi_{on}C_{lab}^{i-1} + (1 - f_{auto})f_{fol}GPP^i, \quad (3)$$

$$C_{roo}^i = (1 - \theta_{roo})C_{roo}^{i-1} + (1 - f_{auto})(1 - f_{fol})(1 - f_{lab})f_{roo}GPP^i, \quad (4)$$

$$C_{woo}^i = (1 - \theta_{woo})C_{woo}^{i-1} + (1 - f_{auto})(1 - f_{fol})(1 - f_{lab})(1 - f_{roo})GPP^i, \quad (5)$$

$$C_{lit}^i = (1 - (\theta_{lit} + \theta_{min})e^{\Theta T^{i-1}})C_{lit}^{i-1} + \theta_{roo}C_{roo}^{i-1} + \Phi_{off}C_{fol}^{i-1}, \quad (6)$$

$$C_{som}^i = (1 - \theta_{som}e^{\Theta T^{i-1}})C_{som}^{i-1} + \theta_{woo}C_{woo}^{i-1} + \theta_{min}e^{\Theta T^{i-1}}C_{lit}^{i-1}, \quad (7)$$

102 where T^{i-1} is the daily mean temperature, Ψ represents the meteorological driving data used in the GPP function and
 103 Φ_{on}/Φ_{off} are functions controlling leaf-on and leaf-off. The model parameters used in equations (1) to (7) are included
 104 in the appendix in table 3. DALEC2 differs from the original DALEC in that it can be parameterised for both deciduous and
 105 evergreen sites with Φ_{on} and Φ_{off} being able to reproduce the phenology of either type of site. The full details of this version
 106 of DALEC can be found in Bloom and Williams (2015).

107 2.3. 4D-Var

108 Following the approach of Smith et al. (2011) for three-dimensional variational data assimilation, we consider the discrete
109 nonlinear dynamical system given by

$$\mathbf{z}_i = \mathbf{f}_{i-1 \rightarrow i}(\mathbf{z}_{i-1}, \mathbf{p}_{i-1}), \quad (8)$$

110 where $\mathbf{z}_i \in \mathbb{R}^n$ is the state vector at time t_i , $\mathbf{f}_{i-1 \rightarrow i}$ is the nonlinear model operator propagating the state at time t_{i-1} to
111 time t_i for $i = 1, 2, \dots, N$ and $\mathbf{p}_{i-1} \in \mathbb{R}^q$ is a vector of q model parameters at time t_{i-1} . For DALEC2 the state vector
112 $\mathbf{z}_i = (C_{lab}^i, C_{for}^i, C_{roo}^i, C_{woo}^i, C_{lit}^i, C_{som}^i)^T$, with the parameters shown in table 3. The model parameters are not updated by the
113 nonlinear model operator, therefore the evolution of the parameters is given by,

$$\mathbf{p}_i = \mathbf{p}_{i-1}, \quad (9)$$

114 for $i = 1, 2, \dots, N$. We define the new vector \mathbf{x} by joining the parameter vector \mathbf{p} with the model state vector \mathbf{z} , giving us the
115 augmented state vector

$$\mathbf{x} = \begin{pmatrix} \mathbf{p} \\ \mathbf{z} \end{pmatrix} \in \mathbb{R}^{q+n}. \quad (10)$$

116 We define the augmented system model by

$$\mathbf{x}_i = \mathbf{m}_{i-1 \rightarrow i}(\mathbf{x}_{i-1}), \quad (11)$$

117 where

$$\mathbf{m}_{i-1 \rightarrow i}(\mathbf{x}_{i-1}) = \begin{pmatrix} \mathbf{p}_{i-1} \\ \mathbf{f}_{i-1 \rightarrow i}(\mathbf{z}_{i-1}, \mathbf{p}_{i-1}) \end{pmatrix} = \begin{pmatrix} \mathbf{p}_i \\ \mathbf{z}_i \end{pmatrix} \in \mathbb{R}^{q+n}. \quad (12)$$

118 The available observations at time t_i are represented by the vector $\mathbf{y}_i \in \mathbb{R}^{r_i}$ which are related to the augmented state vector
119 through the equation

$$\mathbf{y}_i = \mathbf{h}_i(\mathbf{x}_i) + \boldsymbol{\varepsilon}_i, \quad (13)$$

120 where $\mathbf{h}_i : \mathbb{R}^{q+n} \rightarrow \mathbb{R}^{r_i}$ is the observation operator mapping the augmented state vector to observation space and $\boldsymbol{\varepsilon}_i \in \mathbb{R}^{r_i}$
121 represents the observation errors. These errors are usually assumed to be unbiased, Gaussian and serially uncorrelated with
122 known covariance matrices \mathbf{R}_i .

123 We assume that at time t_0 we have an initial estimate to the augmented state, usually referred to as the background vector
124 denoted \mathbf{x}^b . This background is assumed to have unbiased, Gaussian errors with known covariance matrix \mathbf{B} . In 4D-Var
125 we aim to find the initial state that minimises the weighted least squares distance to the background while minimising the
126 weighted least squares distance of the model trajectory to the observations over the time window t_0, \dots, t_N (Lawless, 2013).

127 We do this by finding the state \mathbf{x}_0^a at time t_0 that minimises the cost function

$$J(\mathbf{x}_0) = \frac{1}{2}(\mathbf{x}_0 - \mathbf{x}^b)^T \mathbf{B}^{-1}(\mathbf{x}_0 - \mathbf{x}^b) + \frac{1}{2} \sum_{i=0}^N (\mathbf{y}_i - \mathbf{h}_i(\mathbf{x}_i))^T \mathbf{R}_i^{-1}(\mathbf{y}_i - \mathbf{h}_i(\mathbf{x}_i)), \quad (14)$$

128 subject to the augmented states \mathbf{x}_i satisfying the nonlinear dynamical model (11). The state that minimises the cost function,
129 \mathbf{x}_0^a , is commonly called the analysis. This state is found using a minimisation routine that takes as its input arguments the cost
130 function, the background vector (\mathbf{x}^b) and also the gradient of the cost function given as,

$$\nabla J(\mathbf{x}_0) = \mathbf{B}^{-1}(\mathbf{x}_0 - \mathbf{x}^b) - \sum_{i=0}^N \mathbf{M}_{i,0}^T \mathbf{H}_i^T \mathbf{R}_i^{-1}(\mathbf{y}_i - \mathbf{h}_i(\mathbf{x}_i)) \quad (15)$$

131 where $\mathbf{H}_i = \frac{\partial \mathbf{h}_i(\mathbf{x}_i)}{\partial \mathbf{x}_i}$ is the linearized observation operator and $\mathbf{M}_{i,0} = \mathbf{M}_{i-1} \mathbf{M}_{i-2} \cdots \mathbf{M}_0$ is the tangent linear model with $\mathbf{M}_i =$
132 $\frac{\partial \mathbf{m}_{i-1 \rightarrow i}(\mathbf{x}_i)}{\partial \mathbf{x}_i}$. In practice $\nabla J(\mathbf{x}_0)$ is calculated using the method of Lagrange multipliers as shown in Lawless (2013). We can
133 rewrite the cost function and its gradient to avoid the sum notation as,

$$J(\mathbf{x}_0) = \frac{1}{2}(\mathbf{x}_0 - \mathbf{x}^b)^T \mathbf{B}^{-1}(\mathbf{x}_0 - \mathbf{x}^b) + \frac{1}{2}(\hat{\mathbf{y}} - \hat{\mathbf{h}}(\mathbf{x}_0))^T \hat{\mathbf{R}}^{-1}(\hat{\mathbf{y}} - \hat{\mathbf{h}}(\mathbf{x}_0)) \quad (16)$$

134 and

$$\nabla J(\mathbf{x}_0) = \mathbf{B}^{-1}(\mathbf{x}_0 - \mathbf{x}^b) - \hat{\mathbf{H}}^T \hat{\mathbf{R}}^{-1}(\hat{\mathbf{y}} - \hat{\mathbf{h}}(\mathbf{x}_0)), \quad (17)$$

135 where,

$$\hat{\mathbf{y}} = \begin{pmatrix} \mathbf{y}_0 \\ \mathbf{y}_1 \\ \vdots \\ \mathbf{y}_N \end{pmatrix}, \quad \hat{\mathbf{h}}(\mathbf{x}_0) = \begin{pmatrix} \mathbf{h}_0(\mathbf{x}_0) \\ \mathbf{h}_1(\mathbf{m}_{0 \rightarrow 1}(\mathbf{x}_0)) \\ \vdots \\ \mathbf{h}_N(\mathbf{m}_{0 \rightarrow N}(\mathbf{x}_0)) \end{pmatrix}, \quad \hat{\mathbf{R}} = \begin{pmatrix} \mathbf{R}_{0,0} & \mathbf{R}_{0,1} & \cdots & \mathbf{R}_{0,N} \\ \mathbf{R}_{1,0} & \mathbf{R}_{1,1} & \cdots & \mathbf{R}_{1,N} \\ \vdots & \vdots & \ddots & \vdots \\ \mathbf{R}_{N,0} & \mathbf{R}_{N,1} & \cdots & \mathbf{R}_{N,N} \end{pmatrix} \quad \text{and} \quad \hat{\mathbf{H}} = \begin{pmatrix} \mathbf{H}_0 \\ \mathbf{H}_1 \mathbf{M}_0 \\ \vdots \\ \mathbf{H}_N \mathbf{M}_{N,0} \end{pmatrix}. \quad (18)$$

136 Solving the cost function in this form also allows us to build serial time correlations into the observation error covariance
137 matrix $\hat{\mathbf{R}}$. The off-diagonal blocks of $\hat{\mathbf{R}}$ represent correlations in time between assimilated observations and are usually taken
138 to be zero, in section 2.6 we show how these off-diagonal blocks can be specified.

139 2.4. Implementation and testing of 4D-Var system

140 In our DALEC2 4D-Var scheme we are performing joint parameter and state estimation. The augmented state vector, \mathbf{x}_0 ,
141 corresponds to the vector of the 17 model parameters and 6 initial carbon pool values, which can be found in the appendix in
142 table 3. Here the nonlinear model (DALEC2) only updates the initial carbon pool values when evolving the augmented state
143 vector forward in time with the parameters being held constant. To find the background estimate, \mathbf{x}^b , to the augmented state
144 vector we can either use a previous DALEC2 model forecast estimate of the state of the system for the site (when available)

or use expert elicitation to define likely state and parameter values and ranges for the site. The background vector (\mathbf{x}^b) and its corresponding standard deviations (see table 3) used in this paper were provided from existing runs of the the CARbon DAta-MoDel fraMework (CARDAMOM) (Exbrayat et al., 2015). This is a dataset derived from satellite observations of leaf area index which provides a reasonable first guess to DALEC2 state and parameter values for the Alice Holt research site. In this paper we assimilate observations of daily NEE. From Richardson et al. (2008) the measurement error in observations of daily NEE is between 0.2 to 0.8 $\text{gCm}^{-2}\text{day}^{-1}$. We assume a standard deviation of 0.5 $\text{gCm}^{-2}\text{day}^{-1}$ in the assimilated observations of daily NEE as we found this standard deviation gave the best weighting to the observations in the assimilation algorithm, producing the best results for the forecast of NEE after assimilation.

In order to find the tangent linear model (TLM) for DALEC2 it is necessary to find the derivative of the model at each time step with respect to the 17 model parameters and the 6 carbon pools. We use the AlgoPy automatic differentiation package (Walter and Lehmann, 2013) in Python to calculate the TLM at each time step. This package uses forward mode automatic differentiation to calculate the derivative of the model. In the following tests we use a diagonal approximation to the background and observation error covariance matrices so that, $\mathbf{B}_{diag} = \text{diag}(\boldsymbol{\sigma}_b)^2$ and $\hat{\mathbf{R}}_{diag} = \text{diag}(\boldsymbol{\sigma}_o)^2$, where $\boldsymbol{\sigma}_b$ is the vector of background standard deviations found in table 3 and $\boldsymbol{\sigma}_o$ is the vector of observational standard deviations, for a single observation of NEE $\sigma_o = 0.5 \text{ gCm}^{-2}\text{day}^{-1}$. The minimisation routine used in our data assimilation experiments is the truncated Newton method (Nocedal and Wright, 1999) from the Python package Scipy.optimize (Jones et al., 2001). In sections 2.4.1 to 2.4.3 we show tests of our scheme.

2.4.1. Test of tangent linear model

We can have confidence that our implementation of the TLM for DALEC2 is correct as it passes the following relevant tests (Li et al., 1994). In 4D-Var we assume the tangent linear hypothesis,

$$\mathbf{m}_{0 \rightarrow i}(\mathbf{x}_0 + \gamma \delta \mathbf{x}_0) \approx \mathbf{m}_{0 \rightarrow i}(\mathbf{x}_0) + \gamma \mathbf{M}_{i,0} \delta \mathbf{x}_0, \quad (19)$$

where $\delta \mathbf{x}_0$ is a perturbation of the initial augmented state \mathbf{x}_0 and γ is a parameter controlling the size of this perturbation. The validity of this assumption depends on how nonlinear the model is, the length of the assimilation window and the size of the augmented state perturbation $\delta \mathbf{x}_0$. We can test this by rearranging equation (19) to find,

$$\frac{\|\mathbf{m}_{0 \rightarrow i}(\mathbf{x}_0 + \gamma \delta \mathbf{x}_0) - \mathbf{m}_{0 \rightarrow i}(\mathbf{x}_0)\|}{\|\gamma \mathbf{M}_{i,0} \delta \mathbf{x}_0\|} \rightarrow 0, \quad (20)$$

as $\gamma \rightarrow 0$ (here we are using the Euclidean norm). Figure 2 shows equation (20) plotted for DALEC2 with i fixed at 731 days, a fixed 5% perturbation $\delta \mathbf{x}_0$ and values of γ approaching zero. Figure 2 shows that the TLM behaves as expected for values of γ approaching 0. This was also tested for different choices of \mathbf{x}_0 and sizes of perturbation with similar results.

It is also useful to show how the TLM behaves over a time window to see how the error in the TLM grows as we evolve the

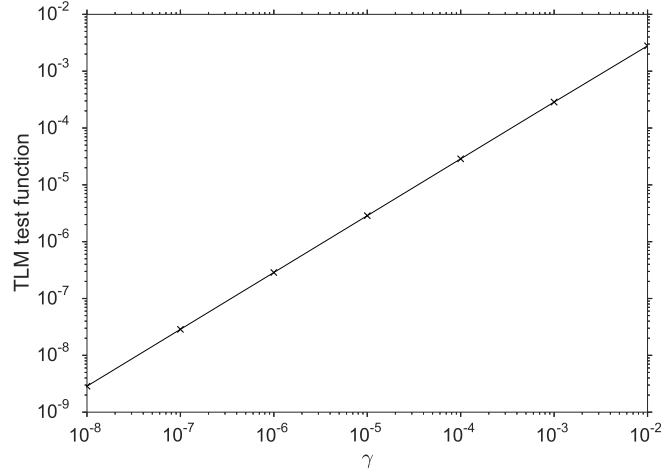


Figure 2: Plot of the tangent linear model test function (equation (20)) for DALEC2, for a TLM evolving the augmented state 731 days forward in time and a fixed 5% perturbation, $\delta \mathbf{x}_0$.

172 augmented state further forward in time. We again rearrange equation (19) with an additional error term to find,

$$\text{percentage error in TLM} = \frac{\|m_{0 \rightarrow i}(\mathbf{x}_0 + \gamma \delta \mathbf{x}_0) - m_{0 \rightarrow i}(\mathbf{x}_0) - \gamma \mathbf{M}_{i,0} \delta \mathbf{x}_0\|}{\|\gamma \mathbf{M}_{i,0} \delta \mathbf{x}_0\|} \times 100. \quad (21)$$

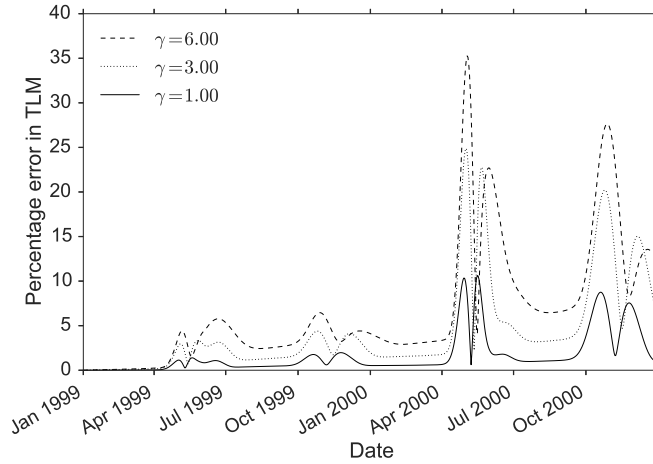


Figure 3: Plot of the percentage error in the tangent linear model (equation (21)) for DALEC2 when evolving the model state forward over a period of two years with three different values of γ and a fixed 5% perturbation $\delta \mathbf{x}_0$.

173 In figure 3 we can see that the TLM for DALEC2 performs well after being run forward a year with less than a 7% error for
 174 all values of γ . By the second year we see some peaks in the error in spring and autumn. This is due to leaf on and leaf off
 175 functions in the TLM going out of phase with the nonlinear DALEC2. At these peaks the error reaches a maximum at 35%
 176 then coming back to around 10% before growing again in the autumn. For this reason we present results using a one year
 177 assimilation window in this paper.

178 2.4.2. Test of adjoint model

179 The adjoint model we have implemented for DALEC2 passes correctness tests. For the TLM $\mathbf{M}_{i,0}$ and its adjoint $\mathbf{M}_{i,0}^T$ we
180 have the identity

$$< \mathbf{M}_{i,0} \delta \mathbf{x}_0, \mathbf{M}_{i,0} \delta \mathbf{x}_0 > = < \delta \mathbf{x}_0, \mathbf{M}_{i,0}^T \mathbf{M}_{i,0} \delta \mathbf{x}_0 > \quad (22)$$

181 for any inner product $<, >$ and perturbation $\delta \mathbf{x}_0$. This is derived from the adjoint identity (Lawless, 2013). Using the
182 Euclidean inner product, equation (22) is equivalent to

$$(\mathbf{M}_{i,0} \delta \mathbf{x}_0)^T (\mathbf{M}_{i,0} \delta \mathbf{x}_0) = \delta \mathbf{x}_0^T (\mathbf{M}_{i,0}^T \mathbf{M}_{i,0} \delta \mathbf{x}_0). \quad (23)$$

183 We evaluated the left hand side and right hand side of this identity for differing values of \mathbf{x}_0 and size of perturbation $\delta \mathbf{x}_0$ and
184 showed that they were equal to machine precision.

185 2.4.3. Gradient test

186 The 4D-Var system we have developed passes tests for the gradient of the cost function (Navon et al., 1992). In the imple-
187 mentation of the cost function and its gradient we regularise the problem using a variable transform (Freitag et al., 2010). For
188 the cost function J and its gradient ∇J we can show that we have implemented ∇J correctly using the identity,

$$f(\alpha) = \frac{|J(\mathbf{x}_0 + \alpha \mathbf{b}) - J(\mathbf{x}_0)|}{\alpha \mathbf{b}^T \nabla J(\mathbf{x}_0)} = 1 + O(\alpha), \quad (24)$$

189 where \mathbf{b} is a vector of unit length and α is a parameter controlling the size of the perturbation. For small values of α not too
190 close to machine precision we should have $f(\alpha)$ close to 1. Figure 4a shows $f(\alpha)$ for a 365 day assimilation window with
191 $\mathbf{b} = \mathbf{x}_0 / \|\mathbf{x}_0\|^{-1}$, we can see that $f(\alpha) \rightarrow 1$ as $\alpha \rightarrow 0$, as expected until $f(\alpha)$ gets too close to machine zero at order $\alpha = 10^{-11}$.
192 This was also tested with \mathbf{b} in different directions and similar results obtained.

193 We can also plot $|f(\alpha) - 1|$, where we expect $|f(\alpha) - 1| \rightarrow 0$ as $\alpha \rightarrow 0$. In figure 4b we have plotted $|f(\alpha) - 1|$ for the same
194 conditions as in figure 4a, we can see that $|f(\alpha) - 1| \rightarrow 0$ as $\alpha \rightarrow 0$, as expected (before $|f(\alpha) - 1|$ gets too close to machine
195 precision at order $\alpha = 10^{-8}$). This gives us confidence that the gradient of the cost function is implemented correctly.

196 2.5. Including correlations in the background error covariance matrix

197 As discussed in section 1, including correlations in \mathbf{B} impacts how information from assimilated observations is spread
198 between different types of analysis variables (Bannister, 2008). We explored a number of different methods in order to
199 include parameter-state correlations in \mathbf{B} . In this paper we present a method using a set of ecological dynamical constraints,
200 based on expert judgement, on model parameters and state variables from Bloom and Williams (2015). Bloom and Williams
201 (2015) show that implementing these constraints in a Metropolis Hastings MCMC data assimilation routine improves results

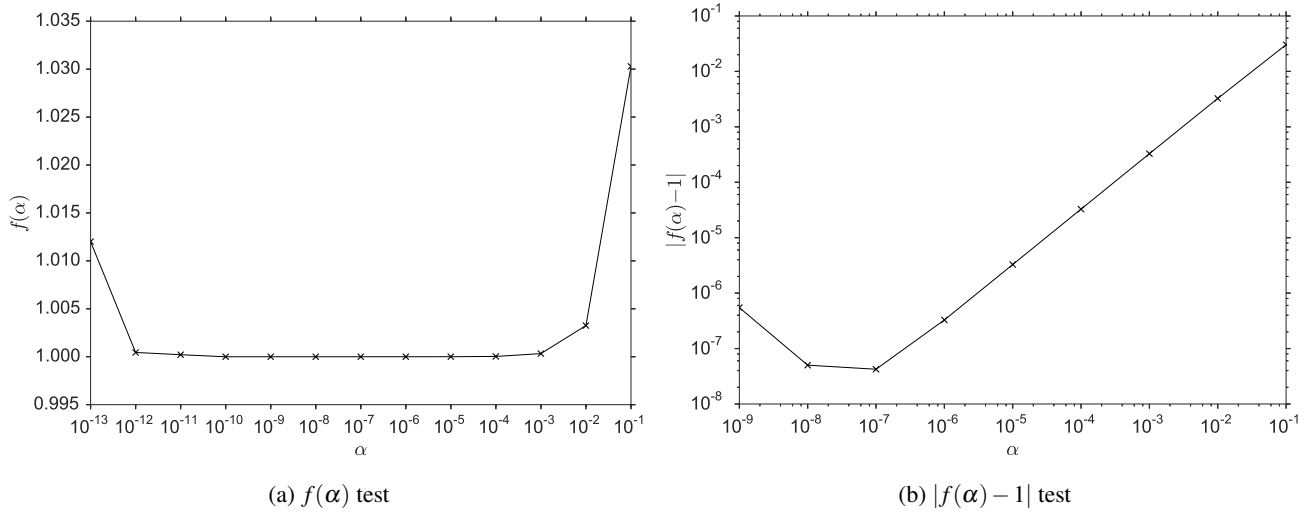


Figure 4: Tests of the gradient of the cost function for a 365 day assimilation window with $\mathbf{b} = \mathbf{x}_0 \|\mathbf{x}_0\|^{-1}$.

significantly. The constraints impose conditions on carbon pool turnover and allocation ratios, steady state proximity and growth and the decay of model carbon pools.

In order to create a correlated background error covariance matrix, \mathbf{B}_{corr} , using these constraints we create an ensemble of state vectors which we then take the covariance of to give us \mathbf{B}_{corr} . To create this ensemble we use the following procedure:

1. Draw a random augmented state vector, \mathbf{x}_i , from the multivariate truncated normal distribution described by

$$\mathbf{x}_i \sim \mathcal{N}(\mathbf{x}^b, \mathbf{B}_{diag}), \quad (25)$$

where \mathbf{B}_{diag} is the diagonal matrix described in section 2.4 and \mathbf{X} is bound by the parameter and state ranges given in table 3 in the appendix.

2. Test this \mathbf{x}_i with the ecological dynamical constraints (requiring us to run the DALEC2 model using this state).
3. If \mathbf{x}_i passes it is added to our ensemble, else it is discarded.

Once we have a full ensemble we then take the covariance of the ensemble to find \mathbf{B}_{corr} . We chose an ensemble size of 1500 as using a larger ensemble did not appear to change values of correlations significantly. In figure 5 we have plotted the correlation matrix or normalised error covariance matrix associated with \mathbf{B}_{corr} . This matrix includes both positive and negative correlations between parameter and state variables, with correlations of 1 down the diagonal between variables of the same quantity as expected. The largest positive off-diagonal correlation is 0.42 between f_{lab} and C_{lab} . This makes physical sense as f_{lab} is the parameter controlling the amount of GPP allocated to the labile carbon pool, C_{lab} .

2.6. Specifying serial correlations in the observation error covariance matrix

The observation error covariance matrix does not only represent the instrumentation error for an observation but also the error in the observation operator (mapping the model state to the observation) and representativity error (error arising from the

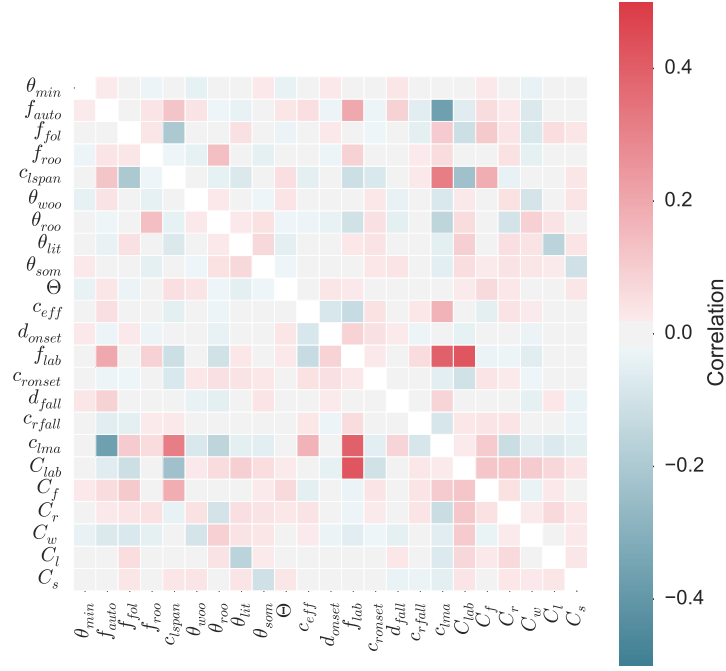


Figure 5: Background error correlation matrix created using method in section 2.5. Here the correlation scale for off-diagonal values ranges from -0.5 to 0.5 with the correlation along the diagonal being 1. For explanation of parameter and state variable symbols see table 3.

model being unable resolve the spatial and temporal scales of the observations). These other sources of error represented in $\hat{\mathbf{R}}$ can also lead to correlations between observation errors (Waller et al., 2014). Errors in NEE observations come from different sources such as instrument errors, sampled ecosystem structure from the variable footprint of the flux tower and turbulent conditions (when there is low turbulence and limited air mixing NEE is underestimated). These errors due to turbulence can still have effect even after u^* filtering (Papale et al., 2006). Due to this dependence on atmospheric conditions we expect the errors in observations of NEE to be serially correlated, as the atmospheric signal itself is serially correlated (Daley, 1992). If we were assimilating half hourly observations of NEE we would expect stronger correlations between observation errors, as atmospheric conditions are more constant at this time scale, with correlations between observation errors getting weaker with lower frequency observations. Although some studies suggest that the correlation between NEE measurement errors on the scale of a day is negligible (Lasslop et al., 2008), it is also likely that error in the observation operator and representativity error will lead to observation error correlations for NEE (Waller et al., 2014).

In section 2.3 we have re-written the 4D-Var cost function in equation (16) in order to allow the specification of serial observation error correlations in our assimilation scheme. These serial correlations are represented by the off-diagonal blocks of $\hat{\mathbf{R}}$. In work carried out with spatial correlations it has been shown that the structure of the correlation is not critical and that it is better to include some estimate of error correlation structure in the observation error covariance matrix than wrongly assume that errors are independent (Stewart et al., 2013; Healy and White, 2005). As a first attempt we try including temporal correlations on the scale of the observation frequency. We adapt the simple Gaussian model found in Järvinen et al. (1999) (a second order autoregressive correlation function was also tested but is not presented here). The correlation r between 2

observations at times t_1 and t_2 is given as,

$$r = \begin{cases} a \exp \left[\frac{-(t_1 - t_2)^2}{\tau^2} \right] + (1 - a) \delta_{t_1 - t_2} & |t_1 - t_2| \leq \eta \\ 0 & \eta < |t_1 - t_2| \end{cases}, \quad (26)$$

where τ is the e-folding time, a controls the strength of correlation, δ is the Kronecker delta and η is the cut off time after which the correlation between two observation errors is zero. We have incorporated a cut off for correlations between observation errors as the assumed correlation length scale for the assimilated observations is short. This cut off along with the form of correlation function using the Kronecker delta helps ensure $\hat{\mathbf{R}}$ is positive definite and therefore invertible, as required in the assimilation process. The standard deviation assumed in the observations of NEE is $0.5 \text{ gCm}^{-2}\text{day}^{-1}$ as described in section 2.4.

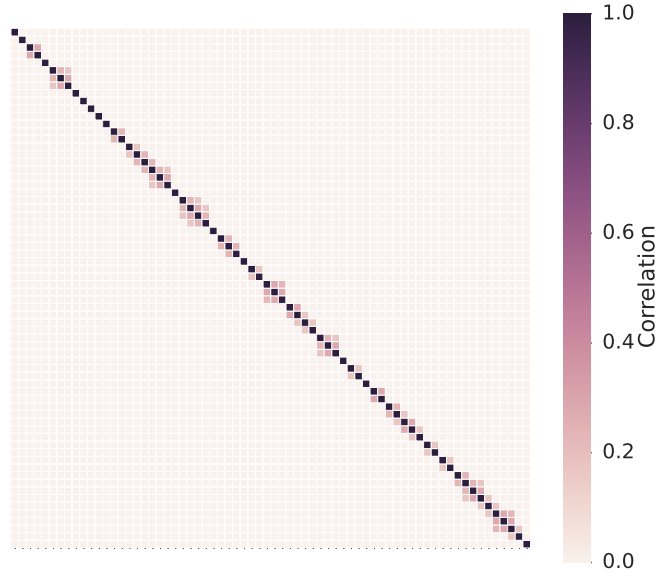


Figure 6: Observation error correlation matrix for the 67 observations used in assimilation created using method in section 2.6 with $\tau = 4$, $a = 0.3$ and $\eta = 4$.

Figure 6 shows the correlation matrix for $\hat{\mathbf{R}}$ created using equation (26). There are 67 NEE observations in this one year assimilation window, these observations are not all on adjacent days and this is evident in the structure of $\hat{\mathbf{R}}$. The effect of the short e-folding time chosen here ($\tau = 4$) provides the desired structure.

3. Results

3.1. Experiments

In the following sections we present the results of four experiments where we vary the representations of \mathbf{B} and $\hat{\mathbf{R}}$ while assimilating the same NEE observations in the window from the beginning of January 1999 to the end of December 1999. As shown in figure 3 the performance of the tangent linear model deteriorates after the first year. We then forecast the NEE

over the next 14 years (Jan 2000 - Dec 2013) and compare with the observed data. Using this shorter analysis window with a long forecast allows us to see the effect of including correlations in the error statistics more clearly. These experiments are outlined in table 1 where \mathbf{B}_{diag} and $\hat{\mathbf{R}}_{diag}$ are the diagonal matrices of the parameter and state variances and the observations variances respectively and \mathbf{B}_{corr} and $\hat{\mathbf{R}}_{corr}$ are the matrices as specified in section 2.5 and section 2.6 respectively.

Experiment	\mathbf{B}_{diag}	$\hat{\mathbf{R}}_{diag}$	\mathbf{B}_{corr}	$\hat{\mathbf{R}}_{corr}$
A	×	×		
B		×	×	
C	×			×
D			×	×

Table 1: The combination of error covariance matrices used in each data assimilation experiment.

3.2. Experiment A

In this experiment \mathbf{B}_{diag} and $\hat{\mathbf{R}}_{diag}$ were used in the assimilation as described in section 3.1. Because these contain no correlations this experiment forms the baseline by which the subsequent results from assimilation experiments are judged.

Figure 7a shows assimilation and forecast results for NEE. We can see that assimilating the observations of NEE has improved the background with the analysis trajectory (green line) fitting well with the observations during the assimilation window (Jan 1999- Dec 1999). The analysis trajectory then diverges in the forecast (Jan 2000 - Dec 2013). This can be seen more clearly in figure 8a, where there is an over prediction of respiration in the winter and the seasonal cycle does not match that of the observations.

To see how well the forecast performs after assimilation we show a scatter plot of modelled NEE against observed NEE in figure 9b. From table 2 the predictions have a Root-Mean-Square Error (RMSE) of $4.22 \text{ gCm}^{-2}\text{day}^{-1}$ and a bias of $-0.3 \text{ gCm}^{-2}\text{day}^{-1}$ for the forecast of NEE, whereas the analysis (Jan 1999 - Dec 1999) has a RMSE of $1.36 \text{ gCm}^{-2}\text{day}^{-1}$ and a bias of $-0.03 \text{ gCm}^{-2}\text{day}^{-1}$. The background trajectory meanwhile has a RMSE of $3.86 \text{ gCm}^{-2}\text{day}^{-1}$ and a bias of $-1.60 \text{ gCm}^{-2}\text{day}^{-1}$ in the analysis window (Jan 1999 - Dec 1999) and the same RMSE of $3.86 \text{ gCm}^{-2}\text{day}^{-1}$ but a bias of $-1.36 \text{ gCm}^{-2}\text{day}^{-1}$ during the forecast period (Jan 2000 - Dec 2013). Although using \mathbf{B}_{diag} and $\hat{\mathbf{R}}_{diag}$ in the assimilation has considerably reduced the RMSE in the analysis period, it has also increased the RMSE in the forecast of NEE. However it has reduced the bias in the model forecast considerably from $-1.36 \text{ gCm}^{-2}\text{day}^{-1}$ to $-0.3 \text{ gCm}^{-2}\text{day}^{-1}$. The bias in the background is due to the background model predicting less negative values of NEE than observed (i.e. above the 1:1 line shown in figure 9a). This leads to considerably worse results for the background trajectory than the analysis and its forecast for total forest carbon uptake.

276 3.3. Experiment B

277 Here \mathbf{B}_{corr} (as defined in section 2.5) and $\hat{\mathbf{R}}_{diag}$ are used in the assimilation. Figure 7b shows assimilation and forecast
 278 results for NEE. In figure 8b we can see that the forecast performs considerably better than in experiment A, with the analysis
 279 trajectory no longer over predicting winter respiration and matching the observed seasonal cycle of NEE more closely in the
 280 forecast period (Jan 2000 - Dec 2013). From figure 9c and table 2 we see that the forecast RMSE has almost halved (now
 281 $2.56 \text{ gCm}^{-2}\text{day}^{-1}$) with a reduction in bias also, now $-0.2 \text{ gCm}^{-2}\text{day}^{-1}$. In comparison using \mathbf{B}_{corr} in the assimilation
 282 very slightly degrades the fit for the analysis (Jan 1999 - Dec 1999), with a RMSE of $1.42 \text{ gCm}^{-2}\text{day}^{-1}$ and a bias of
 283 $-0.04 \text{ gCm}^{-2}\text{day}^{-1}$, as shown in table 2.

284 As discussed in section 1 previous work has shown the importance of specifying parameter-state correlations when using
 285 variational data assimilation for joint parameter and state estimation (Smith et al., 2009). Although in 4D-Var some correlation
 286 structure is added implicitly as \mathbf{B}_{diag} is evolved through time in experiment A, observations near the beginning of the window
 287 (before significant correlations develop in \mathbf{B}_{diag}) will not be spread in a multivariate way. The correlations developed by
 288 the implicit evolution of \mathbf{B}_{diag} may also not include important physical relationships between variables. Therefore by not
 289 specifying these correlations in experiment A we allow the parameter and state variables to attain unrealistic values in order
 290 to find the best fit to the observations in the analysis window (Jan 1999 - Dec 1999), leading to the divergence seen in the
 291 forecast (1999-2014) in experiment A.

292 We can see the effect that including correlations in \mathbf{B} has on the analysis update in figure 10. For some variables including
 293 correlations in \mathbf{B} has had a large impact on the analysis update after assimilation. This is particularly clear for the f_{lab}
 294 parameter. The largest positive off-diagonal correlation in \mathbf{B}_{corr} is between C_{lab} and f_{lab} , with f_{lab} also having a large positive
 295 correlation with c_{lma} as shown in section 2.5. The effect of these correlations has been to change the analysis increment for
 296 f_{lab} from being slightly positive in experiment A to being strongly negative by following the analysis update of its correlated
 297 variables C_{lab} and c_{lma} . From figure 10 we can also see some of the reasons for the improved fit to the observations in
 298 experiment B. We see that the parameters controlling day of leaf on (d_{onset}) has been updated differently in comparison to
 299 experiment A, with day of leaf on now being later in the year, again this is due to the included correlations in \mathbf{B} . This allows the
 300 forecast to better match the observed seasonal cycle of NEE. The forecast is also no longer over predicting winter respiration
 301 as in experiment A. From figure 10 we see that the main parameters controlling ecosystem respiration in NEE (f_{auto} , θ_{lit} ,
 302 θ_{som} , Θ) have been reduced in comparison with experiment A, leading to an improved fit to observations in experiment B. In
 303 experiment A we also had an over prediction of peak carbon uptake in summer which has been improved in this experiment.
 304 From figure 10 we see that one of the parameters controlling the magnitude of gross primary productivity (c_{eff}) has been
 305 decreased in comparison to experiment A. This leads to less extreme predictions of peak summer carbon uptake than in
 306 experiment A.

307 The added constraint provided by the correlations in \mathbf{B}_{corr} reduces the likelihood that parameter and state variables will attain
 308 unrealistic values in order to fit the assimilated observations. Although this has led to a slightly degraded fit to the observations

309 in the analysis window (Jan 1999 - Dec 1999) it has also significantly improved the fit to observations for the forecast (Jan
310 2000 - Dec 2013).

311 3.4. Experiment C

312 Here we use \mathbf{B}_{diag} and $\hat{\mathbf{R}}_{corr}$ (as defined in section 2.6) in the assimilation. Results shown in figure 7c and 8c appear similar
313 to those in section 3.2 however there are some differences. From table 2 and figure 9d we see a slight reduction in RMSE
314 for the forecast (now $4.09 \text{ gCm}^{-2}\text{day}^{-1}$) in comparison with experiment A. As in experiment B the fit to the observations
315 in the analysis window (Jan 1999 - Dec 1999) is very slightly degraded as the added correlations in $\hat{\mathbf{R}}_{corr}$ act to reduce the
316 weight of the observations in the assimilation (Järvinen et al., 1999). The changes seen when using $\hat{\mathbf{R}}_{corr}$ in the assimilation
317 are less than when using \mathbf{B}_{corr} as the correlations specified in $\hat{\mathbf{R}}_{corr}$ are on a short timescale and smaller than those in \mathbf{B}_{corr} . In
318 figure 10 we can see that the changes between experiment A and C in the analysis increment are much less than when using
319 \mathbf{B}_{corr} .

320 We also expect that specifying time correlations in $\hat{\mathbf{R}}$ will help when assimilating other less frequently sampled data streams
321 along with NEE as the serial correlations reduce the weight given to the mean of the more frequently sampled observations
322 (here NEE) and also reduce the information content of these more frequently sampled observations (Järvinen et al., 1999;
323 Daley, 1992), meaning that less frequently sampled data streams can have more impact on the assimilation.

324 3.5. Experiment D

325 In the final experiment we use \mathbf{B}_{corr} and $\hat{\mathbf{R}}_{corr}$ in the assimilation. Figure 8d and figure 8b shows that using both correlated
326 matrices gives similar results as experiment B when \mathbf{B}_{corr} is used with $\hat{\mathbf{R}}_{diag}$. However using $\hat{\mathbf{R}}_{corr}$ in addition to \mathbf{B}_{corr}
327 provides similar improvements as in experiment C. From table 2 and figure 9e we see the forecast RMSE is slightly reduced
328 again still from results in experiment B to $2.38 \text{ gCm}^{-2}\text{day}^{-1}$. Using both matrices appears to combine the beneficial effects
329 described in both section 3.3 and section 3.4. In figure 10 we can see that the analysis increment is very similar to experiment
330 B.

331 3.6. Summary

332 In our experiments we have shown that both \mathbf{B}_{corr} and $\hat{\mathbf{R}}_{corr}$ have the effect of improving the model forecast of NEE. As it can
333 be difficult to inspect the skill of a certain model by only plotting model trajectories, in figure 11 we show Taylor diagrams
334 displaying a statistical comparison of the four experiment and background analysis (Jan 1999 - Dec 1999) and forecast (Jan
335 2000 - Dec 2013) results with the observations of NEE. Here the radial distances from the origin to the points are proportional
336 to the standard deviations of the observations and modelled observations and the azimuthal positions give the correlation
337 coefficient between the modelled and observed NEE (Taylor, 2001). If a model predicted the observations perfectly it would
338 have a correlation coefficient of 1 and a radial distance matching that of the observations (represented by the dotted line).

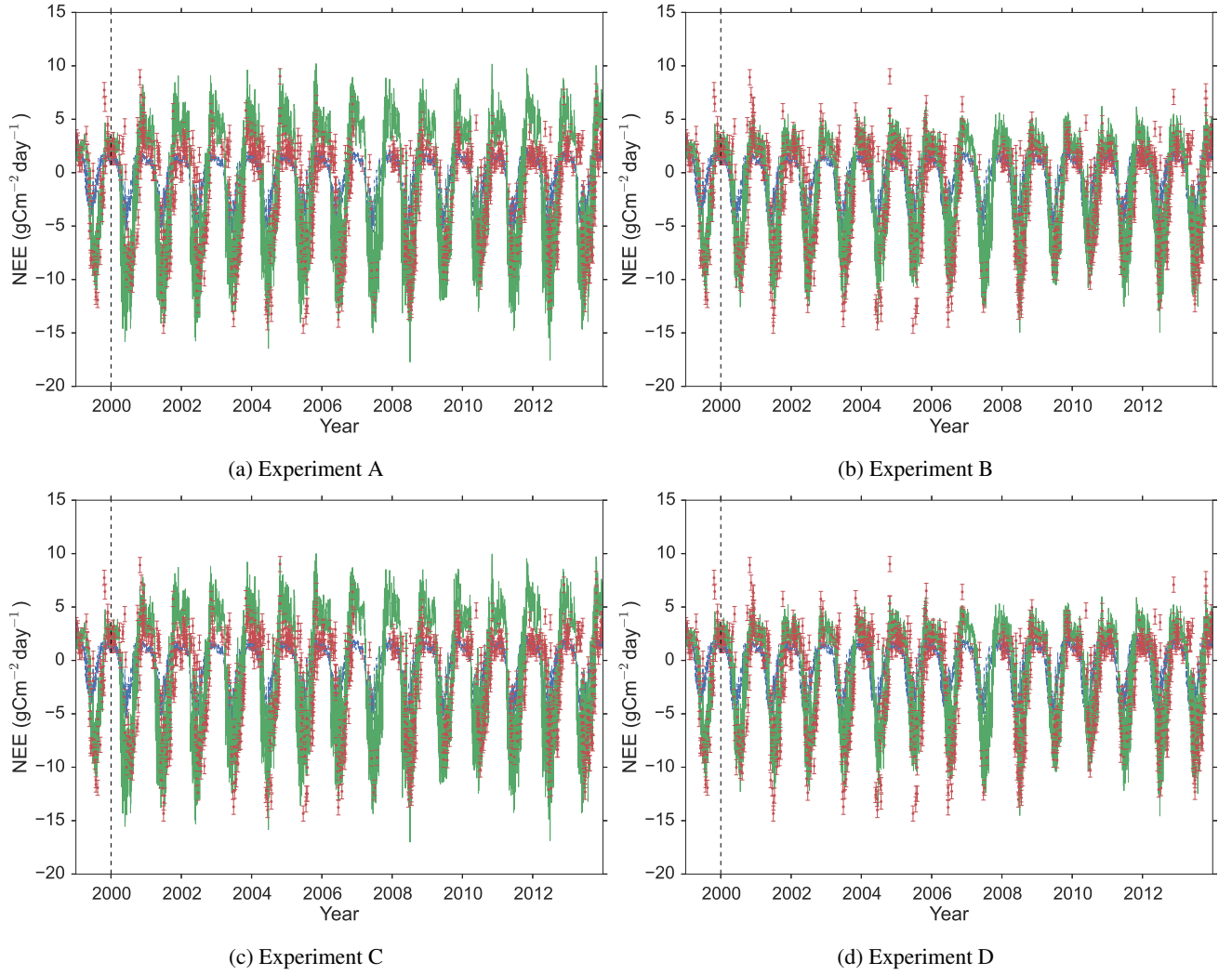


Figure 7: One year assimilation and fourteen year forecast of Alice Holt NEE with DALEC2, blue dotted line: background model trajectory, green line: analysis and forecast after assimilation, red dots: observations from Alice Holt flux site with error bars.

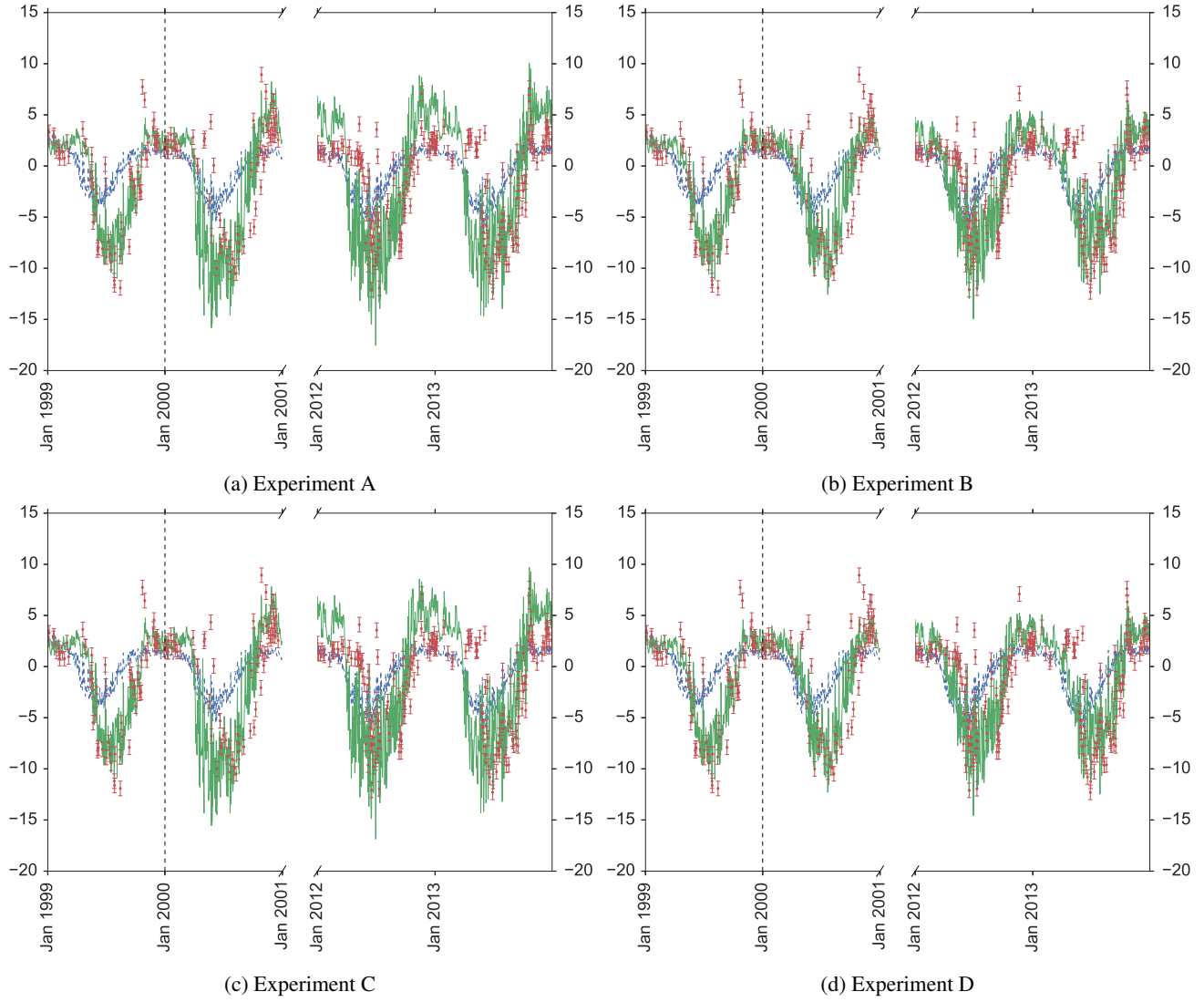


Figure 8: As figure 7 but only showing the first and final two years results from the one year assimilation and fourteen year forecast of Alice Holt NEE with DALEC2, blue dotted line: background model trajectory, green line: analysis and forecast after assimilation, red dots: observations from Alice Holt flux site with error bars.

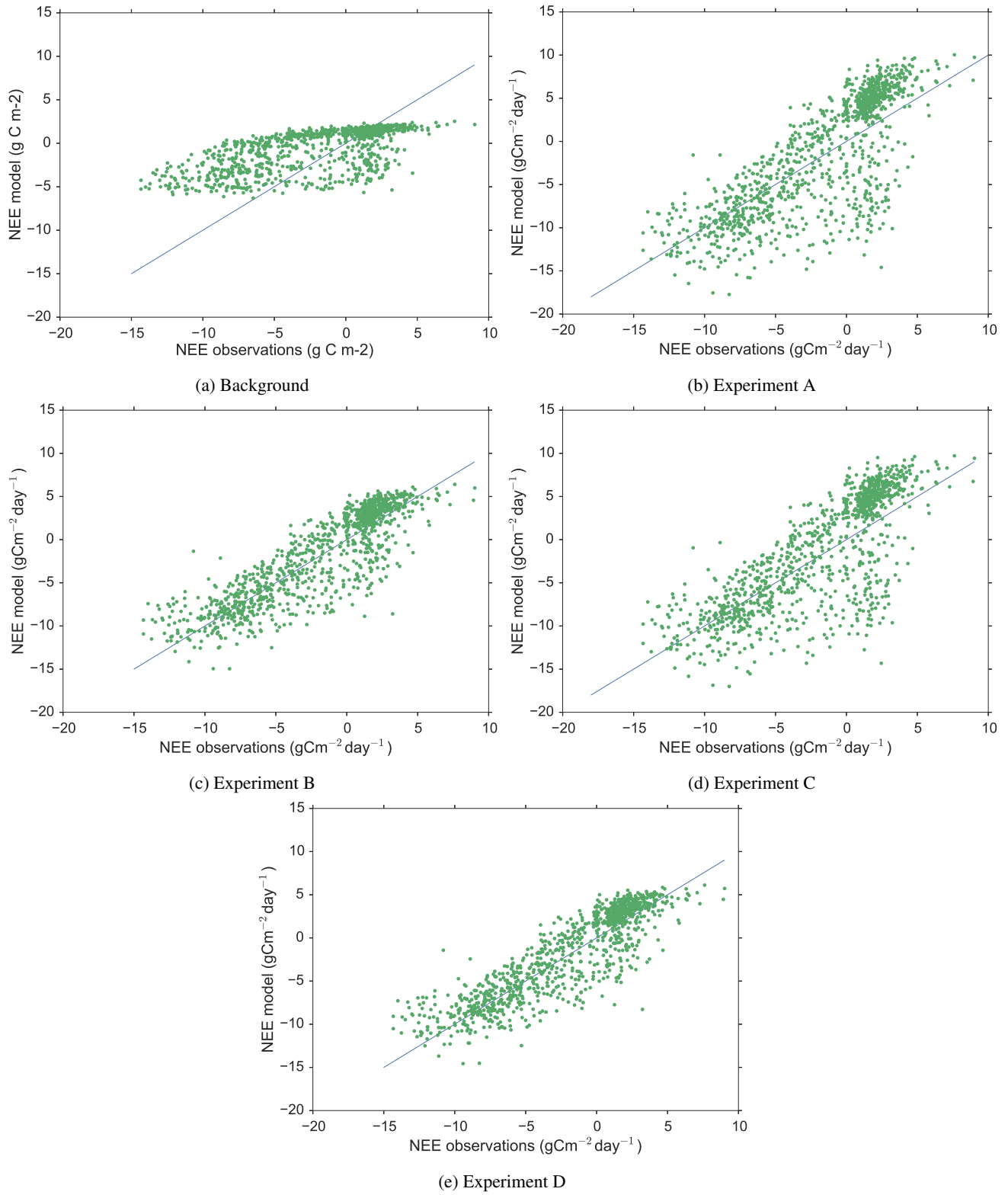


Figure 9: Forecast scatter plot of modelled daily NEE vs. observations for Jan 2000 - Dec 2013 (green dots). Blue line represents the 1-1 line.

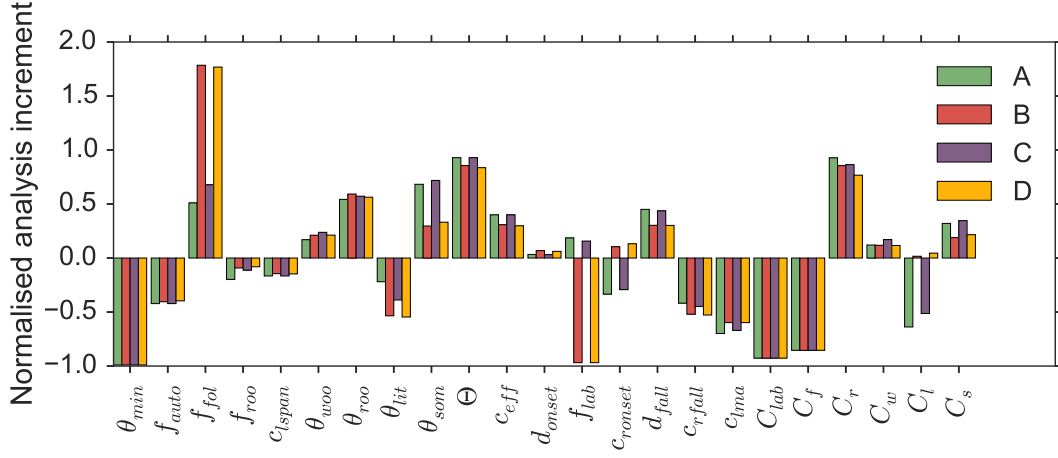


Figure 10: Normalised analysis increment ($\frac{(x^a - x^b)}{x^b}$) for the four experiments. Explanation of parameter and state variable symbols in table 3.

Figure 11a shows that all the experiments give very similar results in the analysis window (Jan 1999 - Dec 1999) with all the experiment points closely grouped on top of each other, whereas figure 11b shows the significant difference between the experiment results in the forecast (Jan 2000 - Dec 2013), with experiments B and D being closer to the dotted line.

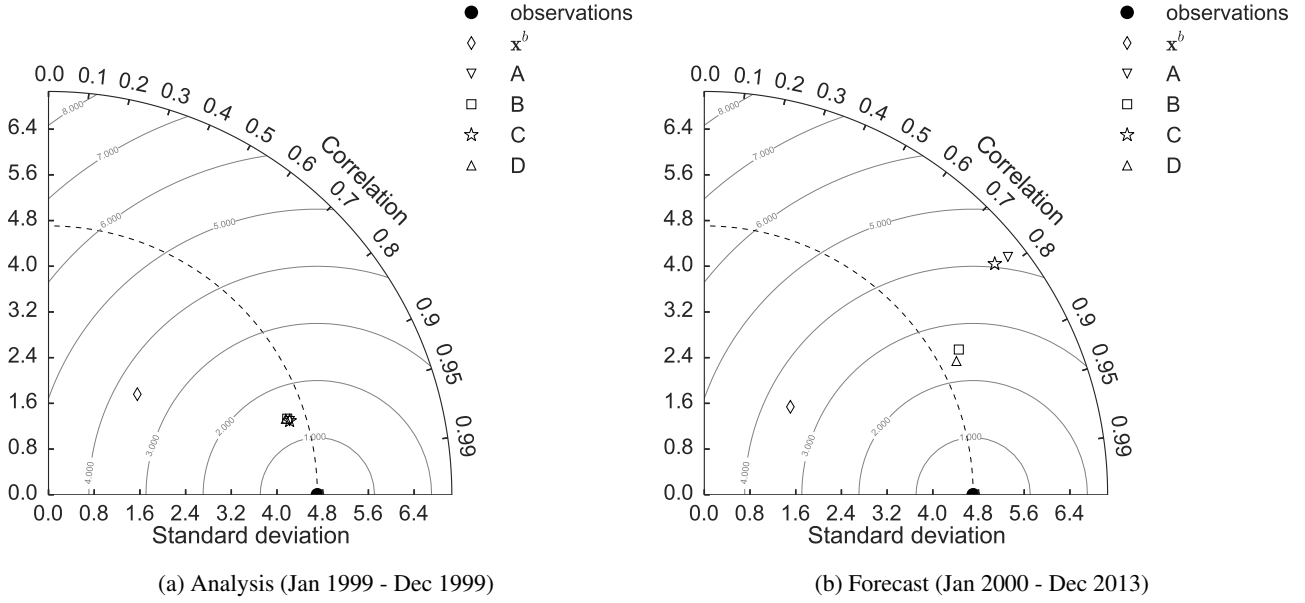


Figure 11: Taylor diagrams displaying statistical comparison of the four experiment and background analysis (Jan 1999 - Dec 1999) and forecast (Jan 2000 - Dec 2013) results with observations of NEE ($\text{gCm}^{-2}\text{day}^{-1}$). The dotted line represents the standard deviation of the observations and the contours represent values of constant root mean square error between model and observations.

4. Discussion

In this paper we have implemented the DALEC2 functional ecology model in a 4D-Var data assimilation scheme, building an adjoint of the DALEC2 model and applying rigorous tests to our scheme. Using 4D-Var can provide much faster assimilation results than MCMC techniques as we have knowledge of the derivative of the model. For our experiments the 4D-Var routine

Analysis (Jan 1999 - Dec 1999)			
Experiment	RMSE ($\text{gCm}^{-2}\text{day}^{-1}$)	Bias ($\text{gCm}^{-2}\text{day}^{-1}$)	Correlation coefficient
Background	3.86	-1.60	0.70
A	1.36	-0.03	0.96
B	1.42	-0.04	0.95
C	1.37	-0.09	0.96
D	1.43	-0.09	0.95
Forecast (Jan 2000 - Dec 2013)			
Experiment	RMSE ($\text{gCm}^{-2}\text{day}^{-1}$)	Bias ($\text{gCm}^{-2}\text{day}^{-1}$)	Correlation coefficient
Background	3.86	-1.36	0.66
A	4.22	-0.30	0.79
B	2.56	-0.20	0.87
C	4.09	-0.51	0.78
D	2.38	-0.33	0.88

Table 2: Analysis (Jan 1999 - Dec 1999) and forecast (Jan 2000 - Dec 2013) results for experiments and background when judged against observed NEE.

has taken in the order of 10^2 function evaluations to converge to a minimum, whereas MCMC techniques using the same model take in the order of 10^8 function evaluations (Bloom and Williams, 2015). However, we do assume that the statistics of the problem are Gaussian whereas MCMC techniques do not. We have shown that 4D-Var is a valid tool for improving the DALEC2 model estimate of NEE and that even when assimilating only a single year of NEE observations we can improve the forecast significantly. In practice this type of data assimilation routine would be run in cycling mode running the analysis from the first year as the background for the second then iterating this until all data is assimilated (Moodey et al., 2013). However, here our aim is to investigate the effect of specifying correlations in background and observation error statistics on the forecast of NEE. We have therefore assimilated just one year of NEE observations and produced a long 14 year forecast in order to see more clearly the effect of including these correlations on the forecast when judging against observations. The observations of daily NEE from the Alice Holt flux site are quite variable year to year, peak summer uptake varies from $-14.35 \text{ gCm}^{-2}\text{day}^{-1}$ to $-9.04 \text{ gCm}^{-2}\text{day}^{-1}$, and therefore provide a reasonable test for the ability of the DALEC2 model forecast, especially over a 14 year period.

We then considered the nature of background and observation errors. The effect of specifying parameter-state correlations in the background information and serial correlations between the observation errors was explored.

The technique presented here to specify \mathbf{B}_{corr} has been shown to have significantly improved forecasts of NEE over using a diagonal representation of \mathbf{B} . In section 3.3 we discuss how the correlations in \mathbf{B}_{corr} impact the analysis update for the parameter and state variables (see figure 10) causing the seasonal cycle of carbon uptake and magnitude of fluxes to fit more

363 closely with the observations than when using a diagonal \mathbf{B} in the assimilation algorithm. These results agree with those
 364 of Smith et al. (2009) where the importance of specifying parameter-state correlations when performing joint parameter and
 365 state estimation with variational data assimilation was shown. The method for specifying \mathbf{B}_{corr} in this paper used a series of
 366 ecological dynamical constraints taken from Bloom and Williams (2015). In cases where these type of constraints are not
 367 available there are other methods to build correlations into \mathbf{B} . One technique we also tested (not presented here) to create a
 368 correlated \mathbf{B} involved evolving an ensemble of state vectors over the length of the chosen assimilation window using the model
 369 (DALEC2) and then taking the covariance of the evolved ensemble. This gave us a \mathbf{B} with parameter-state and state-state
 370 correlations, but no parameter-parameter correlations as the parameters are not updated by the model. Using the \mathbf{B} created
 371 with this method also improved assimilation results significantly over using a diagonal \mathbf{B} . A larger number of different tests
 372 were run using different background vectors and variances and it was found that specifying some form of correlation structure
 373 in \mathbf{B} always made an improvement to the results of the assimilation. As this work has only considered a single deciduous site,
 374 it would be useful to apply the techniques detailed here for an evergreen site. Evergreen ecosystems usually have less extreme
 375 seasonal variation, it will therefore be of interest to see if a similar improvement for evergreen ecosystem forecast results is
 376 found when using a \mathbf{B}_{corr} created using the same method.

377 The purpose of this exercise was to see how well we could forecast NEE while also investigating the effect of including
 378 correlations between error statistics. It was not an attempt to recover all the parameters and state variables with a high level
 379 of accuracy. However, it is still instructive to look at these values and compare with data where available. In Meir et al.
 380 (2002) an observed range is given for leaf mass per area (c_{lma}) for the Alice Holt flux site of between 40 to 80 gCm^{-2} . The
 381 background value for c_{lma} in our experiments is 128.5 gCm^{-2} . When using diagonal error covariance matrices in experiment
 382 A we find a value of 38.7 gCm^{-2} for c_{lma} after assimilation which is almost within the range given by Meir et al. (2002). In
 383 experiment D when using error covariance matrices including correlations c_{lma} has a value of 51.6 gCm^{-2} after assimilation,
 384 this is well within the observed range given by Meir et al. (2002) and again shows an improvement when using the correlated
 385 error covariance matrices. From observations made by Forest Research we also have estimates to the above and below ground
 386 woody carbon pool (C_{woo}) at the start of 1999 with an observed value of 14258 gCm^{-2} , it is not clear how uncertain this
 387 estimate is. The background value for C_{woo} in our experiments is 6506 gCm^{-2} . When using diagonal error covariance
 388 matrices in experiment A we find a value of 7291 gCm^{-2} for C_{woo} , an increase but still far away from the observed estimate.
 389 In experiment D when using error covariance matrices including correlations C_{woo} has a value of 7262 gCm^{-2} a similar result
 390 as experiment A. Here the assimilation has not been able to recover a value of C_{woo} similar to that of the observed estimate.
 391 This is expected as we are assimilating observations of daily NEE only and NEE is a product of Gross Primary Productivity
 392 (GPP) and Total ecosystem respiration (RT), ($NEE = RT - GPP$), with neither GPP nor RT being direct functions of C_{woo} .
 393 Therefore it is not possible to recover an accurate value of C_{woo} as the assimilated observations are not significantly impacted
 394 by large changes in this state variable (i.e. equifinality), this result is also found in Fox et al. (2009). This also explains why
 395 we are able to recover a reasonable value of c_{lma} from the assimilation, as from equation (1) we can see that c_{lma} is one of the
 396 input arguments taken by GPP. The function calculating GPP will therefore be sensitive to variations in the c_{lma} parameter

397 and so assimilating observations of NEE should help to constrain this parameter.

398 In numerical weather prediction it has been shown that including correlations in \mathbf{R} can help improve data assimilation results
399 (Weston et al., 2014; Stewart et al., 2013). However the specified correlations have most commonly been satellite interchannel
400 correlations with observations errors still being considered independent in time. In this paper we have shown that including
401 correlations between observation errors in time can also improve data assimilation results, here improving the DALEC2
402 model forecast of NEE. We expect including these serial correlations to have an even greater impact when assimilating more
403 than one data stream. When assimilating multiple data streams more frequently sampled observation types (such as NEE)
404 have much more impact on the assimilation than data streams sampled less frequently. Specifying serial correlations between
405 observations of the same type has the effect of reducing the weight given to the mean of the observations (Järvinen et al.,
406 1999), thus allowing less frequent data streams to have more impact on the assimilation. Using the form of $\hat{\mathbf{R}}$ given in this
407 paper for specifying serial correlations will also allow us to specify serial correlations between different observation types.
408 When running the DALEC2 model with a day-night time step, instead of the daily time step used for this paper, this will
409 allow us to build in the type of correlations investigated by Baldocchi et al. (2015) between ecosystem respiration and canopy
410 photosynthesis. More work is needed to investigate the effect of including correlations between observations error statistics
411 when assimilating multiple data streams.

412 The $\hat{\mathbf{R}}_{corr}$ presented in this paper has a weak correlation ($\alpha = 0.3$) in time between observations of NEE, this representation
413 of $\hat{\mathbf{R}}_{corr}$ has improved the model forecast of NEE. However other choices of $\hat{\mathbf{R}}_{corr}$ (with stronger correlations between obser-
414 vations) tested for this paper degraded the forecast. This is probably due to the specified correlations being unrealistic and
415 suggests a more diagnostic approach is needed for the calculation of serial correlations in $\hat{\mathbf{R}}$. One option would be to adapt
416 the Desroziers et al. (2005) diagnostic, which has been used successfully in numerical weather prediction for diagnosing
417 observation error correlations for observations taken at the same time (Weston et al., 2014), and extending this technique to
418 diagnose serial correlations. This will form the basis of future work.

419 5. Conclusion

420 Functional ecology and land surface model data assimilation routines largely treat prior estimates of parameter and state
421 uncertainties and observation error statistics as independent and uncorrelated. In this paper we have shown the importance of
422 including estimates to such correlations, especially between background parameter and state error statistics when performing
423 joint parameter and state estimation.

424 When performing joint parameter and state estimation including correlations in the background error covariance matrix sig-
425 nificantly improves the forecast after assimilation, in comparison to using a diagonal representation of \mathbf{B} . Specifying serial
426 time correlations between observation errors in $\hat{\mathbf{R}}$ also improves the forecast and we expect these correlations to have a greater
427 impact when assimilating more than one data stream. More work is needed to investigate the effect of including these corre-

lations when assimilating multiple data streams. The development of a more diagnostic tool for the calculation of the error correlation structure in $\hat{\mathbf{R}}$ is also important.

When including both parameter-state correlations in \mathbf{B} and time correlations between observation errors in $\hat{\mathbf{R}}$ and assimilating only a single year of NEE observations we can forecast 14 years of NEE observations with a root-mean square error of $2.38 \text{ gCm}^{-2}\text{day}^{-1}$ and a correlations coefficient of 0.88. This is a significant 44% reduction in error from the results when using a \mathbf{B} and $\hat{\mathbf{R}}$ with no specified correlations of $4.22 \text{ gCm}^{-2}\text{day}^{-1}$ and a correlation coefficient of 0.79.

6. Acknowledgements

This work was funded by the UK Natural Environment Research Council (NE/K00705X/1) with a CASE award from the UK Forestry Commission. T. Quaife's contribution funded by the National Centre for Earth Observation. We are grateful to Luke Smallman for providing the background information used in the experiments detailed in this paper.

References

- Bacour, C., Peylin, P., MacBean, N., Rayner, P.J., Delage, F., Chevallier, F., Weiss, M., Demarty, J., Santaren, D., Baret, F., Berneiller, D., Dufrêne, E., Prunet, P., 2015. Joint assimilation of eddy-covariance flux measurements and FAPAR products over temperate forests within a process-oriented biosphere model. *Journal of Geophysical Research: Biogeosciences*, n/a–n/doi:10.1002/2015JG002966.
- Baldocchi, D., 2008. Turner review no. 15. 'breathing' of the terrestrial biosphere: lessons learned from a global network of carbon dioxide flux measurement systems. *Australian Journal of Botany* 56, 1–26.
- Baldocchi, D., Sturtevant, C., Contributors, F., 2015. Does day and night sampling reduce spurious correlation between canopy photosynthesis and ecosystem respiration? *Agricultural and Forest Meteorology* 207, 117–126. doi:10.1016/j.agrformet.2015.03.010.
- Bannister, R.N., 2008. A review of forecast error covariance statistics in atmospheric variational data assimilation. i: Characteristics and measurements of forecast error covariances. *Quarterly Journal of the Royal Meteorological Society* 134, 1951–1970.
- Bauer, P., Thorpe, A., Brunet, G., 2015. The quiet revolution of numerical weather prediction. *Nature* 525, 47–55.
- Bloom, A.A., Williams, M., 2015. Constraining ecosystem carbon dynamics in a data-limited world: integrating ecological "common sense" in a model data fusion framework. *Biogeosciences* 12, 1299–1315. doi:10.5194/bg-12-1299-2015.
- Bonavita, M., Hlm, E., Isaksen, L., Fisher, M., 2015. The evolution of the ecmwf hybrid data assimilation system. *Quarterly Journal of the Royal Meteorological Society*, n/a–n/doi:10.1002/qj.2652.

Braswell, B.H., Sacks, W.J., Linder, E., Schimel, D.S., 2005. Estimating diurnal to annual ecosystem parameters by synthesis of a carbon flux model with eddy covariance net ecosystem exchange observations. *Global Change Biology* 11, 335–355.

Ciais, P., Sabine, C., Bala, G., Bopp, L., Brovkin, V., Canadell, J., Chhabra, A., DeFries, R., Galloway, J., Heimann, M., et al., 2014. Carbon and other biogeochemical cycles, in: *Climate change 2013: the physical science basis. Contribution of Working Group I to the Fifth Assessment Report of the Intergovernmental Panel on Climate Change*. Cambridge University Press, pp. 465–570.

Clayton, A.M., Lorenc, A.C., Barker, D.M., 2013. Operational implementation of a hybrid ensemble/4d-var global data assimilation system at the met office. *Quarterly Journal of the Royal Meteorological Society* 139, 1445–1461. doi:10.1002/qj.2054.

Daley, R., 1992. The Effect of Serially Correlated Observation and Model Error on Atmospheric Data Assimilation. doi:10.1175/1520-0493(1992)120<0164:TE0SC0>2.0.CO;2.

Dee, D., Uppala, S., Simmons, A., Berrisford, P., Poli, P., Kobayashi, S., Andrae, U., Balmaseda, M., Balsamo, G., Bauer, P., et al., 2011. The era-interim reanalysis: Configuration and performance of the data assimilation system. *Quarterly Journal of the Royal Meteorological Society* 137, 553–597.

Delahaies, S., Roulstone, I., Nichols, N., 2013. A regularization of the carbon cycle data-fusion problem, in: *EGU General Assembly Conference Abstracts*, p. 4087.

Desroziers, G., Berre, L., Chapnik, B., Poli, P., 2005. Diagnosis of observation, background and analysis-error statistics in observation space. *Quarterly Journal of the Royal Meteorological Society* 131, 3385–3396.

Exbrayat, J.f., Smallman, T.L., Bloom, A.A., Williams, M., 2015. Using a data-assimilation system to assess the influence of fire on simulated carbon fluxes and plant traits for the Australian continent. *EGU General Assembly* 17, 6421.

Fox, A., Williams, M., Richardson, A.D., Cameron, D., Gove, J.H., Quaife, T., Ricciuto, D., Reichstein, M., Tomelleri, E., Trudinger, C.M., et al., 2009. The reflex project: comparing different algorithms and implementations for the inversion of a terrestrial ecosystem model against eddy covariance data. *Agricultural and Forest Meteorology* 149, 1597–1615.

Freitag, M.A., Nichols, N.K., Budd, C.J., 2010. L1-regularisation for ill-posed problems in variational data assimilation. *Pamm* 10, 665–668. doi:10.1002/pamm.201010324.

Healy, S., White, A., 2005. Use of discrete Fourier transforms in the 1D-Var retrieval problem. *Quarterly Journal of the Royal Meteorological Society* 131, 63–72. doi:10.1256/qj.03.193.

Järvinen, H., Andersson, E., Bouttier, F., 1999. Variational assimilation of time sequences of surface observations with serially correlated errors. *Tellus A* 51, 469–488.

485 Jones, E., Oliphant, T., Peterson, P., et al., 2001. SciPy: Open source scientific tools for Python. URL: <http://www.scipy.org/>. [Online; accessed 2015-12-04].

486

487 Kalnay, E., 2003. Atmospheric modeling, data assimilation, and predictability. Cambridge university press.

488 Kaminski, T., Knorr, W., Schürmann, G., Scholze, M., Rayner, P.J., Zaehle, S., Blessing, S., Dorigo, W., Gayler, V., Giering, R., Gobron, N., Grant, J.P., Heimann, M., Hooker-Stroud, a., Houweling, S., Kato, T., Kattge, J., Kelley, D., Kemp, S., Koffi, E.N., Köstler, C., Mathieu, P.P., Pinty, B., Reick, C.H., Rödenbeck, C., Schnur, R., Scipal, K., Sebald, C.,

489

490

491 Stacke, T., Van Scheltinga, a.T., Vossbeck, M., Widmann, H., Ziehn, T., 2013. The BETHY/JSBACH Carbon Cycle Data Assimilation System: Experiences and challenges. *Journal of Geophysical Research: Biogeosciences* 118, 1414–1426. doi:10.1002/jgrg.20118.

492

493

494 Krinner, G., Viovy, N., de Noblet-Ducoudré, N., Ogée, J., Polcher, J., Friedlingstein, P., Ciais, P., Sitch, S., Prentice, I.C., 2005. A dynamic global vegetation model for studies of the coupled atmosphere-biosphere system. *Global Biogeochemical Cycles* 19, 1–33. doi:10.1029/2003GB002199.

495

496

497 Lasslop, G., Reichstein, M., Kattge, J., Papale, D., 2008. Influences of observation errors in eddy flux data on inverse model parameter estimation. *Biogeosciences Discussions* 5, 751–785.

498

499 Lawless, A.S., 2013. Variational data assimilation for very large environmental problems., in: Cullen, M.J.P., Freitag, M.A., Kindermann, S., Scheichl, R. (Eds.), *Large scale Inverse Problems: Computational Methods and Applications in the Earth Sciences*, Radon series on Computational and Applied Mathematics, De Gruyter. pp. 55–90.

500

501

502 Li, Y., Navon, I.M., Yang, W., Zou, X., Bates, J.R., Moorthi, S., Higgins, R.W., 1994. Four-Dimensional Variational Data Assimilation Experiments with a Multilevel Semi-Lagrangian Semi-Implicit General Circulation Model. *Monthly Weather Review* 122, 966–983. doi:10.1175/1520-0493(1994)122<0966:FDVDAE>2.0.CO;2.

503

504

505 LI-COR, Inc., 2015. EddyPro 6 Help and User's Guide. LI-COR, Inc. Lincoln, NE.

506

507 Lorenc, A.C., Rawlins, F., 2005. Why does 4d-var beat 3d-var? *Quarterly Journal of the Royal Meteorological Society* 131, 3247–3257.

508

509 Meir, P., Kruijt, B., Broadmeadow, M., Barbosa, E., Kull, O., Carswell, F., Nobre, A., Jarvis, P., 2002. Acclimation of photosynthetic capacity to irradiance in tree canopies in relation to leaf nitrogen concentration and leaf mass per unit area. *Plant, Cell & Environment* 25, 343–357.

510

511 Moodey, A.J.F., Lawless, A.S., Potthast, R.W.E., van Leeuwen, P.J., 2013. Nonlinear error dynamics for cycled data assimilation methods. *Inverse Problems* 29, 025002.

512

513 Navon, I., 1998. Practical and theoretical aspects of adjoint parameter estimation and identifiability in meteorology and oceanography. *Dynamics of Atmospheres and Oceans* 27, 55–79.

514

Navon, I.M., Zou, X., Derber, J., Sela, J., 1992. Variational Data Assimilation with an Adiabatic Version of the NMC Spectral Model. *Monthly Weather Review* 120, 1433–1446. doi:10.1175/1520-0493(1992)120<1433:VDAWAA>2.0.CO;2.

Niu, S., Luo, Y., Dietze, M.C., Keenan, T.F., Shi, Z., Li, J., Iii, F.S.C., 2014. The role of data assimilation in predictive ecology. *Ecosphere* 5, art65. doi:10.1890/ES13-00273.1.

Nocedal, J., Wright, S.J., 1999. Numerical Optimization. Springer Science & Business Media.

Papale, D., Reichstein, M., Aubinet, M., Canfora, E., Bernhofer, C., Kutsch, W., Longdoz, B., Rambal, S., Valentini, R., Vesala, T., Yakir, D., 2006. Towards a standardized processing of Net Ecosystem Exchange measured with eddy covariance technique: algorithms and uncertainty estimation. *Biogeosciences* 3, 571–583. doi:10.5194/bg-3-571-2006.

Quaife, T., Lewis, P., De Kauwe, M., Williams, M., Law, B.E., Disney, M., Bowyer, P., 2008. Assimilating canopy reflectance data into an ecosystem model with an Ensemble Kalman Filter. *Remote Sensing of Environment* 112, 1347–1364. doi:10.1016/j.rse.2007.05.020.

Renaud, J., 1997. Automatic differentiation in robust optimization. *AIAA journal* 35, 1072–1079.

Richardson, A.D., Mahecha, M.D., Falge, E., Kattge, J., Moffat, A.M., Papale, D., Reichstein, M., Stauch, V.J., Braswell, B.H., Churkina, G., Kruijt, B., Hollinger, D.Y., 2008. Statistical properties of random {CO₂} flux measurement uncertainty inferred from model residuals. *Agricultural and Forest Meteorology* 148, 38 – 50. doi:http://dx.doi.org/10.1016/j.agrformet.2007.09.001.

Richardson, A.D., Williams, M., Hollinger, D.Y., Moore, D.J., Dail, D.B., Davidson, E.A., Scott, N.A., Evans, R.S., Hughes, H., Lee, J.T., et al., 2010. Estimating parameters of a forest ecosystem c model with measurements of stocks and fluxes as joint constraints. *Oecologia* 164, 25–40.

Smith, P.J., Dance, S.L., Baines, M.J., Nichols, N.K., Scott, T.R., 2009. Variational data assimilation for parameter estimation: application to a simple morphodynamic model. *Ocean Dynamics* 59, 697–708.

Smith, P.J., Dance, S.L., Nichols, N.K., 2011. A hybrid data assimilation scheme for model parameter estimation: Application to morphodynamic modelling. *Computers & Fluids* 46, 436 – 441. doi:http://dx.doi.org/10.1016/j.compfluid.2011.01.010. 10th {ICFD} Conference Series on Numerical Methods for Fluid Dynamics (ICFD 2010).

Stewart, L.M., Dance, S.L., Nichols, N.K., 2013. Data assimilation with correlated observation errors: Experiments with a 1-D shallow water model. *Tellus, Series A: Dynamic Meteorology and Oceanography* 65, 1–14. doi:10.3402/tellusa.v65i0.19546.

Taylor, K.E., 2001. Summarizing multiple aspects of model performance in a single diagram. *Journal of Geophysical Research* 106, 7183. doi:10.1029/2000JD900719.

544 Verbeeck, H., Peylin, P., Bacour, C., Bonal, D., Steppe, K., Ciais, P., 2011. fluxes in Amazon forests: Fusion of eddy
545 covariance data and the ORCHIDEE model. *Journal of Geophysical Research* 116, 1–19. doi:10.1029/2010JG001544.

546 Waller, J.A., Dance, S.L., Lawless, A.S., Nichols, N.K., Eyre, J.R., 2014. Representativity error for temperature and humidity
547 using the Met Office high-resolution model. *Quarterly Journal of the Royal Meteorological Society* 140, 1189–1197.
548 doi:10.1002/qj.2207.

549 Walter, S.F., Lehmann, L., 2013. Algorithmic differentiation in Python with AlgoPy. *Journal of Computational Science* 4,
550 334–344. doi:10.1016/j.jocs.2011.10.007.

551 Weston, P., Bell, W., Eyre, J., 2014. Accounting for correlated error in the assimilation of high-resolution sounder data.
552 *Quarterly Journal of the Royal Meteorological Society* 140, 2420–2429.

553 Wilkinson, M., Eaton, E., Broadmeadow, M., Morison, J., 2012. Inter-annual variation of carbon uptake by a plantation oak
554 woodland in south-eastern england. *Biogeosciences* 9, 5373–5389.

555 Williams, M., Rastetter, E.B., Fernandes, D.N., Goulden, M.L., Shaver, G.R., Johnson, L.C., 1997. Predicting gross primary
556 productivity in terrestrial ecosystems. *Ecological Applications* 7, 882–894.

557 Williams, M., Schwarz, P.A., Law, B.E., Irvine, J., Kurpius, M.R., 2005. An improved analysis of forest carbon dynamics
558 using data assimilation. *Global Change Biology* 11, 89–105.

559 Zobitz, J., Desai, A., Moore, D., Chadwick, M., 2011. A primer for data assimilation with ecological models using markov
560 chain monte carlo (mcmc). *Oecologia* 167, 599–611.

561 Zobitz, J.M., Moore, D.J.P., Quaife, T., Braswell, B.H., Bergeson, A., Anthony, J.a., Monson, R.K., 2014. Joint data as-
562 simulation of satellite reflectance and net ecosystem exchange data constrains ecosystem carbon fluxes at a high-elevation
563 subalpine forest. *Agricultural and Forest Meteorology* 195-196, 73–88. doi:10.1016/j.agrformet.2014.04.011.

Parameter	Description	Background vector (\mathbf{x}^b)	Standard deviation	Range
θ_{min}	Litter mineralisation rate (day^{-1})	9.810×10^{-4}	2.030×10^{-3}	$10^{-5} - 10^{-2}$
f_{auto}	Autotrophic respiration fraction	5.190×10^{-1}	1.168×10^{-1}	$0.3 - 0.7$
f_{fol}	Fraction of GPP allocated to foliage	1.086×10^{-1}	1.116×10^{-1}	$0.01 - 0.5$
f_{roo}	Fraction of GPP allocated to fine roots	4.844×10^{-1}	2.989×10^{-1}	$0.01 - 0.5$
c_{lspan}	Determines annual leaf loss fraction	1.200×10^0	1.161×10^{-1}	$1.0001 - 10$
θ_{woo}	Woody carbon turnover rate (day^{-1})	1.013×10^{-4}	1.365×10^{-4}	$2.5 \times 10^{-5} - 10^{-3}$
θ_{roo}	Fine root carbon turnover rate (day^{-1})	3.225×10^{-3}	2.930×10^{-3}	$10^{-4} - 10^{-2}$
θ_{lit}	Litter carbon turnover rate (day^{-1})	3.442×10^{-3}	3.117×10^{-3}	$10^{-4} - 10^{-2}$
θ_{som}	Soil and organic carbon turnover rate (day^{-1})	1.113×10^{-4}	1.181×10^{-4}	$10^{-7} - 10^{-3}$
Θ	Temperature dependance exponent factor	4.147×10^{-2}	1.623×10^{-2}	$0.018 - 0.08$
c_{eff}	Canopy efficiency parameter	7.144×10^1	2.042×10^1	$10 - 100$
d_{onset}	Leaf onset day (day)	1.158×10^2	6.257×10^0	$1 - 365$
f_{lab}	Fraction of GPP allocated to labile carbon pool	3.204×10^{-1}	1.145×10^{-1}	$0.01 - 0.5$
c_{ronset}	Labile carbon release period (days)	4.134×10^1	1.405×10^1	$10 - 100$
d_{fall}	Leaf fall day (day)	2.205×10^2	3.724×10^1	$1 - 365$
c_{rfall}	Leaf-fall period (days)	1.168×10^2	2.259×10^1	$10 - 100$
c_{lma}	Leaf mass per area (gCm^{-2})	1.285×10^2	6.410×10^1	$10 - 400$
C_{lab}	Labile carbon pool (gCm^{-2})	1.365×10^2	6.626×10^1	$10 - 1000$
C_{fol}	Foliar carbon pool (gCm^{-2})	6.864×10^1	3.590×10^1	$10 - 1000$
C_{roo}	Fine root carbon pool (gCm^{-2})	2.838×10^2	2.193×10^2	$10 - 1000$
C_{woo}	Above and below ground woody carbon pool (gCm^{-2})	6.506×10^3	7.143×10^3	$100 - 10^5$
C_{lit}	Litter carbon pool (gCm^{-2})	5.988×10^2	5.450×10^2	$10 - 1000$
C_{som}	Soil and organic carbon pool (gCm^{-2})	1.936×10^3	1.276×10^3	$100 - 2 \times 10^5$

Table 3: Parameter values and standard deviations for background vector used in experiments.